JOURNAL OF GEOPHYSICAL RESEARCH, VOL. 102, NO. D23, PAGES 28,333–28,351, DECEMBER 20, 1997

On the significance of regional trace gas distributions as derived from aircraft campaigns in PEM-West A and B

D. H. Ehhalt, F. Rohrer, and A. B. Kraus

Institut für Atmosphärische Chemie, Forschungszentrum Jülich, Germany

M. J. Prather

Department of Earth System Science, University of California at Irvine

D. R. Blake and F. S. Rowland

Department of Chemistry, University of California at Irvine

Abstract. With the help of a chemical transport model we calculate the global distributions of three synthetic tracers with uniform emission rates over the continents, zero emissions over the ocean, and constant lifetimes of 5, 20, and 100 days. These distributions serve as a first approximation to those of the lower alkanes and are analyzed in detail for the region between 115°E and 155°E longitude, 0°N and 56°N latitude, within which the Pacific Exploratory Mission-West (PEM-West) A and B campaigns took place. We show that the longitudinally averaged latitude by altitude distributions of the tracers over that domain obtained from sampling the model data along the flight tracks closely represent those obtained from complete averages over the full data sets for the months March and September when the campaigns took place. We further show that for each campaign the modeled distributions closely resemble those measured for ethane and propane, although these distributions change significantly between the two seasons. Taken together, this demonstrates that the average distributions of ethane and propane measured during PEM-West A and B describe reasonably well the true pattern of these gases between 0°N and 50°N latitude and 115°E and 155°E longitude in both seasons, despite incomplete and irregular sampling of that domain. In turn, the measured distributions can be used to test the model, mainly for correct parameterization of transport.

1. Introduction

In the recent past, quite a number of aircraft campaigns have been conducted to study regional air chemistry, and more such campaigns are planned. One product of these campaigns are regional, three-dimensional (3-D) trace gas distributions constructed by averaging in some form over the data collected [cf. *Blake et al.*, 1996].

In this paper we would like to investigate the significance of the distribution so derived. The question arises because the sampling done aboard an aircraft probes the atmosphere usually only along the flight track, one point at a time. For a reasonable geographical coverage of a large domain, sampling over a time period of about 1 month is required. Thus the sampling of the air volume under investigation is always more or less incomplete, resulting in data points or segments of data points disjunct in space and time. The question then is whether these data segments, when pieced together, yield a distribution, which reasonably approaches the true average concentration pattern of the respective trace gas in that domain over the observation period, or whether the data segments are more likely to represent a haphazard collection of momentary local snap shots, whose interpretation requires a careful analysis of each individual event using the momentary, regional wind fields and regional source distributions. For our investigation we use a 3-D global chemical tracer model, the Goddard Institute for Space Studies (GISS) model [*Prather et al.*, 1987], to calculate the distributions of three synthetic tracers with fixed lifetimes of 5, 20, and 100 days and uniform sources over the land surfaces. The domain to be investigated is the western Pacific for which the mean 3-D distributions are derived for March and September. In addition, we derive the synthetic tracer distributions as they result from sampling

Paper number 97JD01498.
0148-0227/97/97JD-01498$09.00

along the actual flight tracks of the PEM-West A and B campaigns, which took place from September 21 to October 17, 1991, and February 7 to March 19, 1994, respectively. Within the model framework we are able to compare these subsampled distributions with those based on continuous sampling everywhere in the domain and to examine in detail their agreement for each season. Finally the distributions of the synthetic model tracers are compared with the measured distributions of ethane and propane, sampled during both campaigns [*Blake et al.*, 1996; *Gregory and Scott*, 1995]. This last comparison provides a test whether the modeled tracer distributions approach reality despite the simplifying assumption made about the source distribution and chemistry of the synthetic tracers. It also provides an indication as to what degree hydrocarbon distributions can serve to validate model simulations. For the present set of synthetic tracers with fixed lifetimes and uniform continental sources, such a comparison mainly tests the treatment of transport in the model.

2. Model Description

The chemical tracer model (CTM) solves the continuity equations for a set of chemically reactive tracers over a global three-dimensional grid. The CTM is adopted from *Prather et al.* [1987]. In the present study the horizontal extension of a grid box is 8° in latitude and 10° in longitude. The atmosphere between the Earth's surface and 10 hPa is divided into nine terrain-following layers (σ-coordinates) which for the global mean surface pressure of dry air equal to 984 hPa have average midpoints of 959, 894, 787, 635, 470, 322, 202, 110, and 40 hPa. The CTM uses a split-operator method to compute the separate effects of advection, dry and wet convection, large-scale diffusion, sources, and chemistry. The three processes of dynamical tracer redistribution are calculated with an 8-hour time step, while the time step for sources and chemistry is 1 hour. The advective transport of tracer is upstream conserving the second-order moments of the tracer distribution [*Prather*, 1986]. The meteorological data which are used as input for the CTM are provided by the GISS general circulation model (GCM II) [*Hansen et al.*, 1983]. This data set contains 8-hour averages of mass flux, pressure fields, and convection frequencies as well as 5-day averages of temperature and detailed convection statistics for 1 year.

Three tracers are introduced into the model. These synthetic tracers have constant lifetimes of 5, 20, and 100 days, respectively, throughout the atmosphere and all seasons. Their source distribution is very simple: a uniform flux of 10^{14} molecules m^{-2} s^{-1} over all land areas between 60°N and 60°S for each of the three tracers, and zero emissions elsewhere, in particular over the ocean. The emissions from coastal surface grid boxes are scaled to the proportion of land contained therein. Thus the synthetic tracers behave like radioactive noble gases. For brevity, they will be called Rn-5, Rn-20, and Rn-100, respectively. Radon, for example, has a lifetime of 5.5 days and essentially continental (though much smaller) sources. In first approximation the tracers also behave like the alkanes, butane, propane, and ethane, which have also essentially continental (but not uniform) sources and comparable (but not constant) lifetimes in the atmosphere. The flux of each synthetic tracer was selected to approximately match the global emission rate of ethane [c.f. *Rudolph*, 1995] and amounts to $7.1 \cdot 10^{11}$ mol yr^{-1}. The model was run for 1 full year so as to approach steady state and was sampled the second year for the tracer distributions, that is, after at least 4 e-folds. In the following, we first present the global distributions of the tracers for March and September as a background. The detailed regional studies of the tracer distribution focus on the western Pacific from 0°N to 56°N latitude and 115°E to 155°E longitude.

The regional intercomparison is restricted to the synthetic tracers with 5 and 20 days lifetime and to propane and ethane. For PEM-West A, *McKeen et al.* [1996] derived a diurnally averaged OH concentration of $3 \cdot 10^6$ cm^{-3} for the lowest 2 km altitude east of Japan. This translates into local lifetimes of 18 and 4 days, respectively, for ethane and propane, since the alkanes are removed from the atmosphere exclusively by the reaction with the hydroxyl radical, OH. Similar lifetimes are expected for PEM-West B because insolation is nearly the same in both seasons, which are just before spring and after fall equinox. Thus the regional lifetimes of the synthetic tracers and the measured alkanes should be reasonably well matched. We note, however, that the average global concentration of OH is only $1 \cdot 10^6 cm^{-3}$ [*Prinn et al.*, 1995] resulting in globally averaged lifetimes of about 10 days for propane and 50 days for ethane. Moreover, the concentration of OH varies strongly with latitude and season. Thus a correct matching of lifetimes would require a latitudinal (seasonal) adjustment. We did not take this option because one of the aims of our calculations is to check whether transport alone acting on a tracer with constant properties leads to significant seasonally changes in its distribution.

3. Results

3.1. Global Distribution

Examples of the modeled distributions of the tracers Rn-5 and Rn-20 are shown in Figures 1 and 2, respectively, which present horizontal contour maps of constant mixing ratio at three different altitudes: the lower part of the planetary boundary layer (lowest model layer), the free troposphere (500 hPa level), and the upper troposphere (200 hPa level) . The latter level reaches into the lower stratosphere at high latitudes. The contour lines represent the mean mixing ratios for

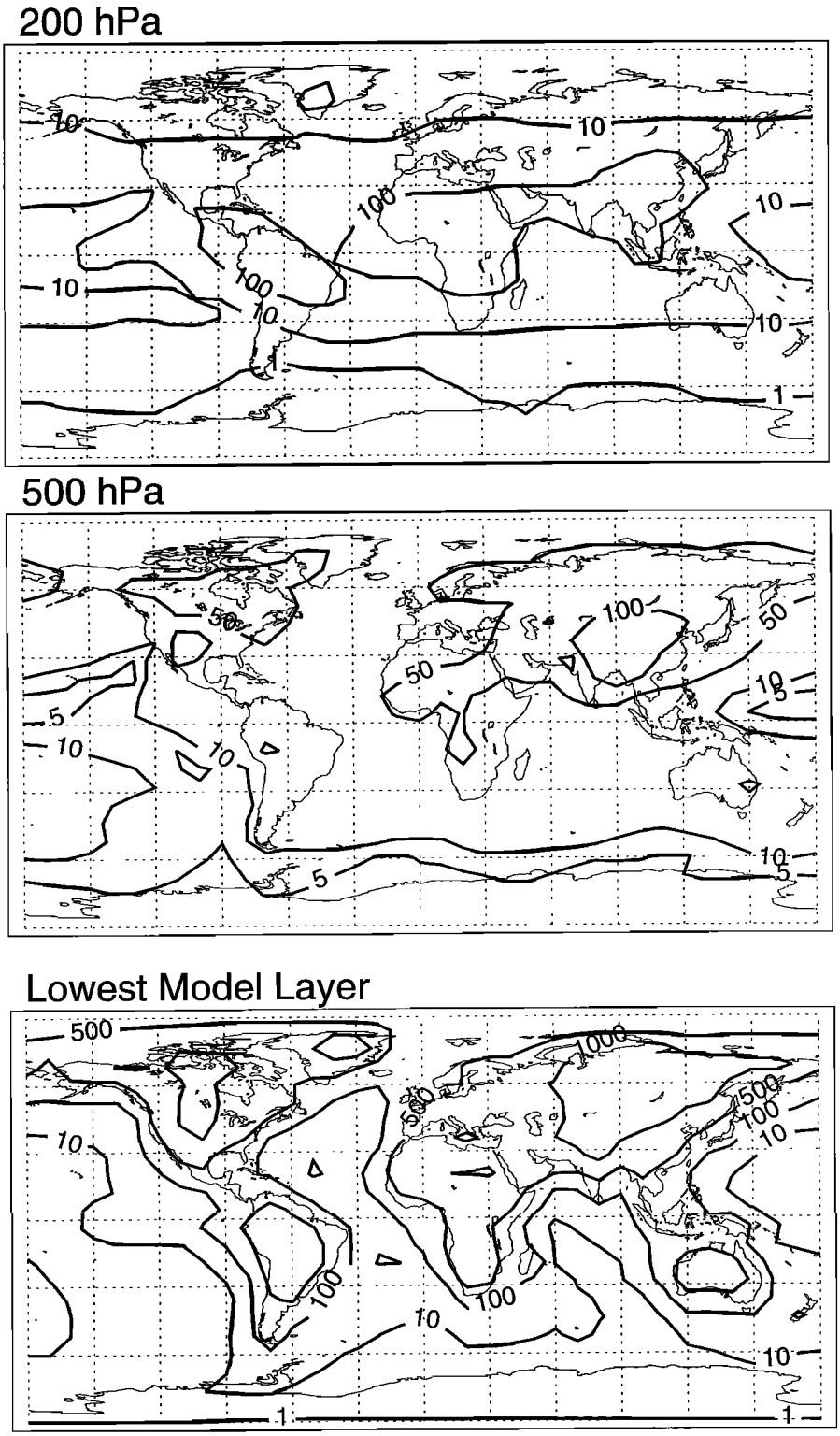

Figure 1. Average global distribution of the tracer Rn-5 during September at the surface, 500 hPa, and 200 hPa. The contours of constant mixing ratio are given in parts per trillion by volume (pptv).

the month of September, roughly the time when the PEM-West A campaign took place. (The corresponding maps for March, when PEM-West B took place, are similar to the ones for September, at least to a cursory glance at the large-scale patterns.)

At the surface level the contours of constant mixing ratio of Rn-5 and Rn-20 clearly follow the outlines of the continents. That correspondence is lost with increasing altitude, where the contour lines at mid and high latitudes align more zonally. Some memory of

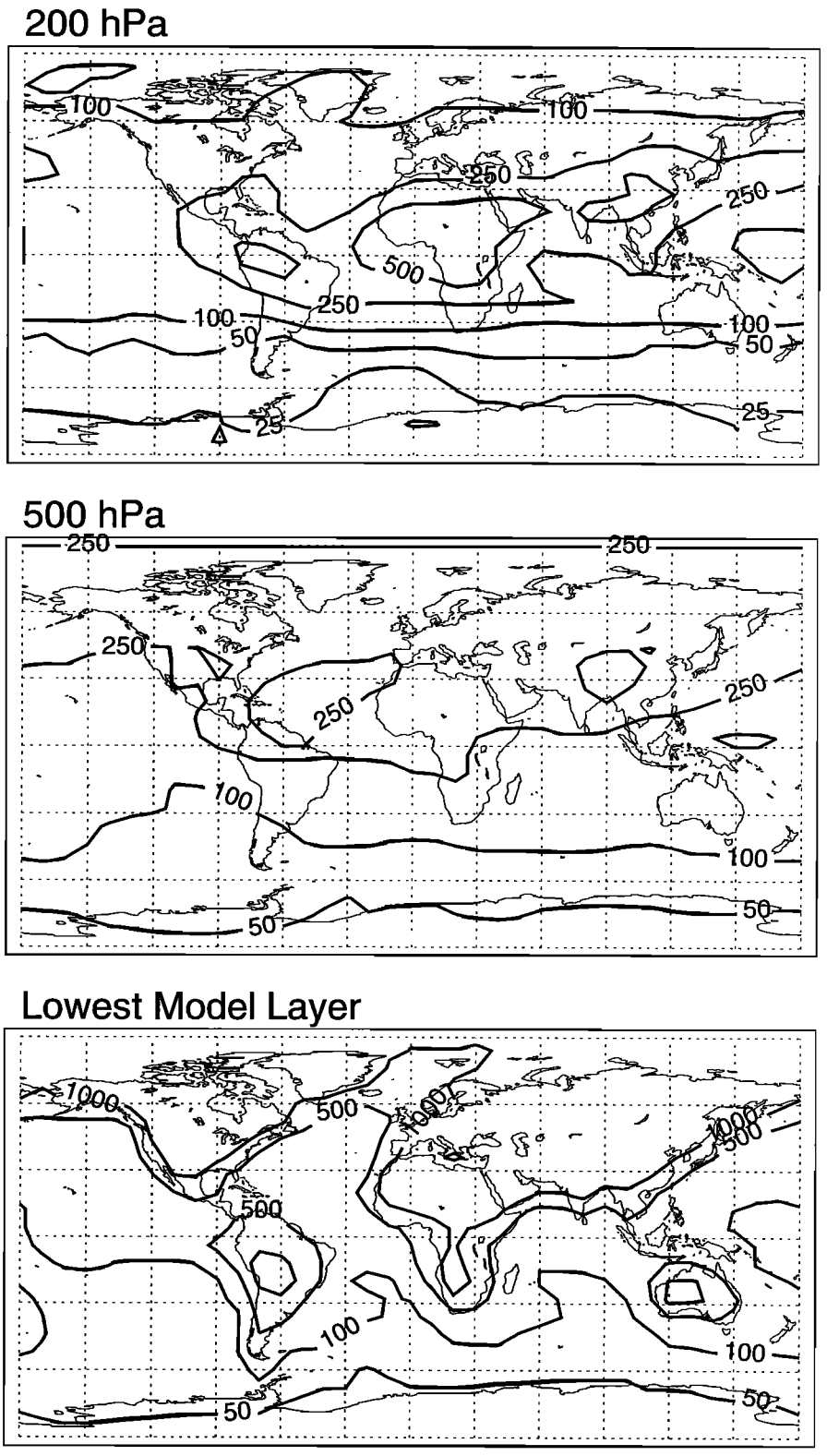

Figure 2. Average global distribution of the tracer Rn-20 during September at the surface, 500 hPa, and 200 hPa level. The contours of constant mixing ratio are given in pptv.

the continental surface source is retained in the contour lines at 200 hPa in the tropics. This pattern is the result of the interplay between the mean zonal wind field, which is stronger at midlatitudes and higher altitudes, and vertical convection, which is stronger in the tropics. Even in September at the end of northern summer, vertical convection over land replenishes the upper troposphere with surface air faster than it does

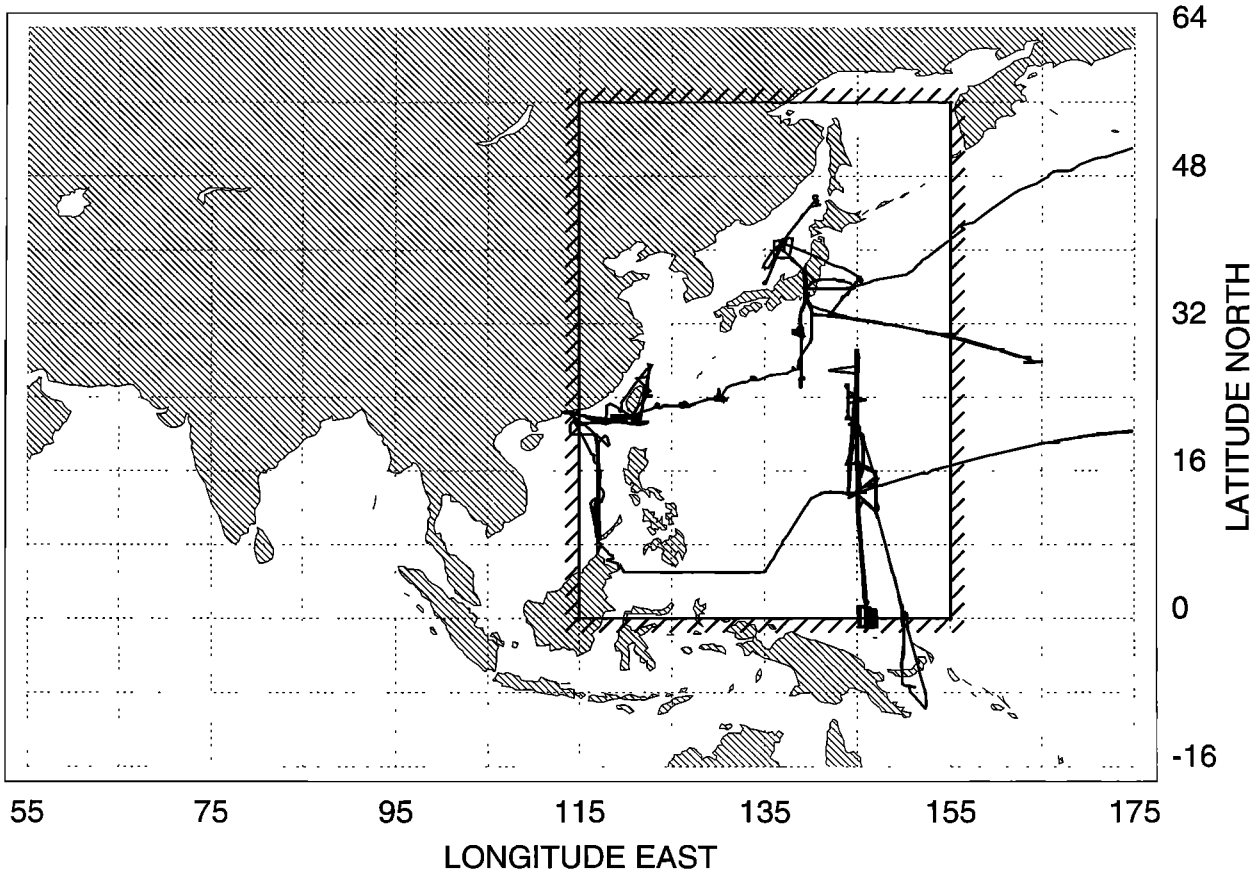

Figure 3. Domain considered in the regional model study of PEM-West A and B. It is outlined by the cross-hatched boundaries. Also shown is the horizontal projection of the flight track during PEM-West B. The thin dashed lines indicate the position of the grid boxes of the CTM model.

the middle troposphere, such that the mixing ratios at 200 hPa are significantly higher than those at 500 hPa above and downwind of the tropical continents for both Rn-5 and Rn-20. At 200 hPa the contours for Rn-20 also show a plume with higher concentrations between 20° and 40°N flowing out from the Asian continent over the western Pacific. Given the values chosen for the mixing ratio contours, this feature is not visible in Figure 1 for Rn-5. Nevertheless, it is present, as evidenced by the regional vertical profiles of Rn-5 in Figure 6. In fact, the features mentioned are more or less common to all three synthetic tracers except that the shorter-lived ones have lower absolute concentrations but larger relative gradients between continents and oceans.

3.2. Regional Distribution Over the Western Pacific

The region of PEM-West B is shown in Figure 3, which includes the CTM grid and the horizontal projection of flight tracks from PEM-West B. We consider the domain enclosing most of the track reaching from 0°N to 56°N and 115°E to 155°E . The flight tracks of PEM-West A are different but cover the same domain [see *Blake et al.*, 1996]. Thus this region encloses most of the measurements made during PEM-West A and B and represents the area with the highest density of experimental data. It includes 28 of the CTM grid squares. The continental coastline cuts diagonally across the domain, such that a larger fraction of the northern grid boxes is affected by the continental surface sources than of the southern ones. Note the uneven distribution of the flight segments over the domain.

Figures 4 to 7 show the monthly mean vertical profiles of Rn-5 and Rn-20 for March and September, respectively, above these 28 grid squares. The profiles are given in 3-D plots of the mixing ratio (in pptv) versus altitude and latitude along the 120°, 130°, 140°, and 150°E longitudes corresponding to the centers of the longitudinal grid (panels a-d, respectively). Also shown are the distributions averaged over all longitudes in the domain (panels e) and an average from sampling the model along the flight tracks of PEM-West B (Figures 4f and 5f) and PEM-West A (Figures 6f and 7f). Mixing ratios are given every kilometer as interpolated between the models vertical levels . In the horizontal direction the values correspond to the CTM grid. Grid boxes sampled during the flight campaigns are marked by a dark end surface. The profiles calculated for February and October, the months, in which the PEM-West B and A campaigns either began or continued, look quite

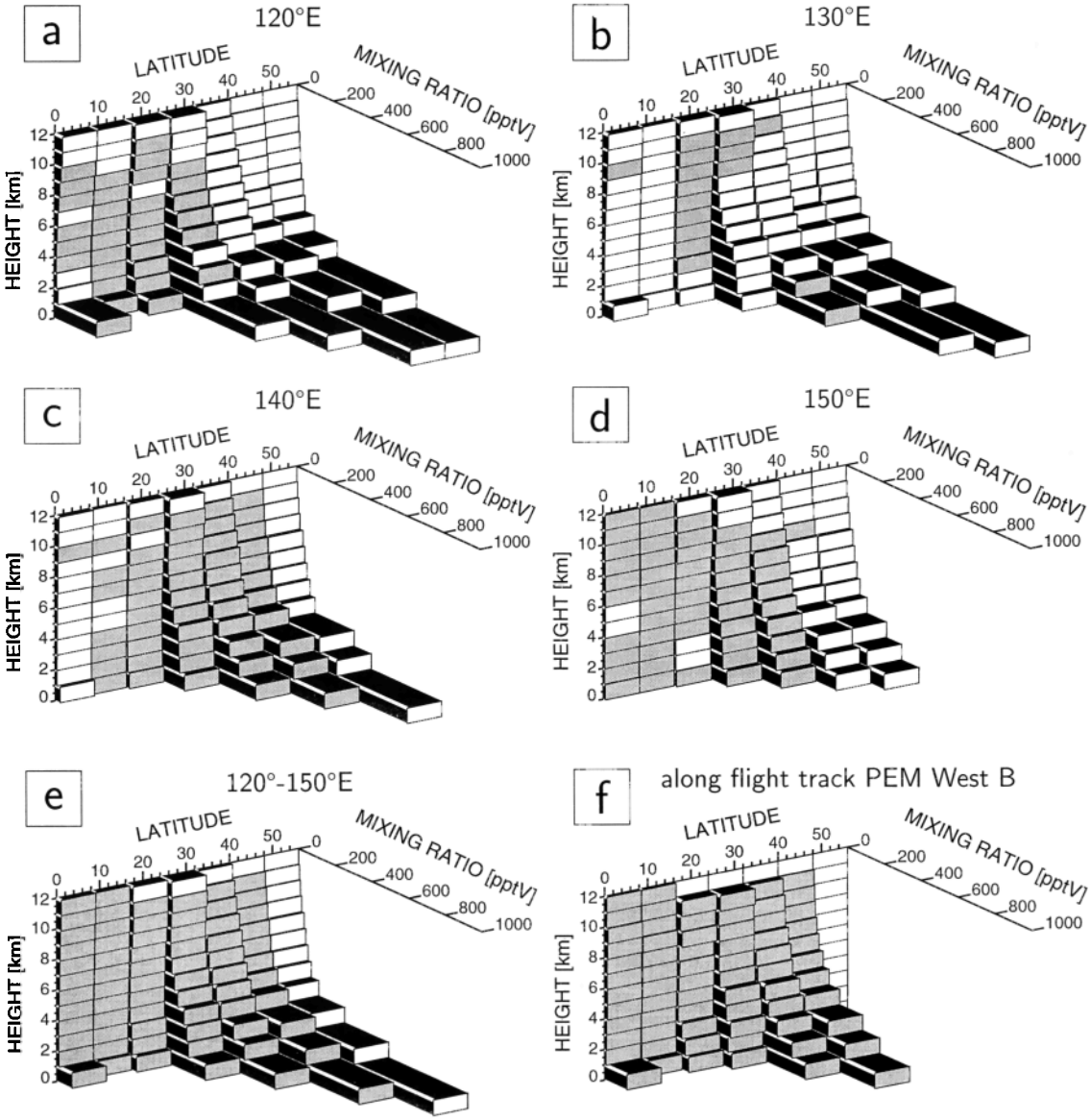

Figure 4. Altitude by latitude plots of the calculated Rn-5 mixing ratios averaged over the month of March along the central longitudes of the grid squares: (a) 120°E, (b) 130°E, (c) 140°E, and (d) 150°E; (e) complete average over all longitudes; (f) average from sampling the monthly averaged distribution along the flight track. Shaded boxes were sampled at least once during the aircraft campaign PEM-West B.

similar to the respective profiles for March and September that are shown here.

For a given month, Rn-5 and Rn-20 exhibit quite clear and similar distribution patterns. Of course, as noted for the global distribution, the absolute mixing ratios are smaller, and the relative gradients larger for the shorter-lived Rn-5.

There are also a number of features that are common to the distributions of March and September, such as the high concentrations in the lower troposphere over land, the decrease in concentrations at all altitudes as the air moves over the ocean, and the tongue of higher concentrations at altitudes above 4 km and all longitudes, between 20° and 40°N latitude during March and between 20° and 50°N during September. This feature was also indicated in the global distribution (Figure 2) and coincides with a band of westerly winds in the middle and upper troposphere. During March the model's westerlies are quite strong with a maximum speed of 65 m s^{-1} at 200 mbar, 32°N, 30°E; during September they are considerably weake r with less than half that wind speed at 200 mbar. Nevertheless, the tongue of higher concentrations appears more strongly expressed in the September distribution. Because of strong convection, the vertical distribution at tropical latitudes is more or less uniform in both months.

The distributions for March and September, however, also show distinct differences. Whereas in March all ver-

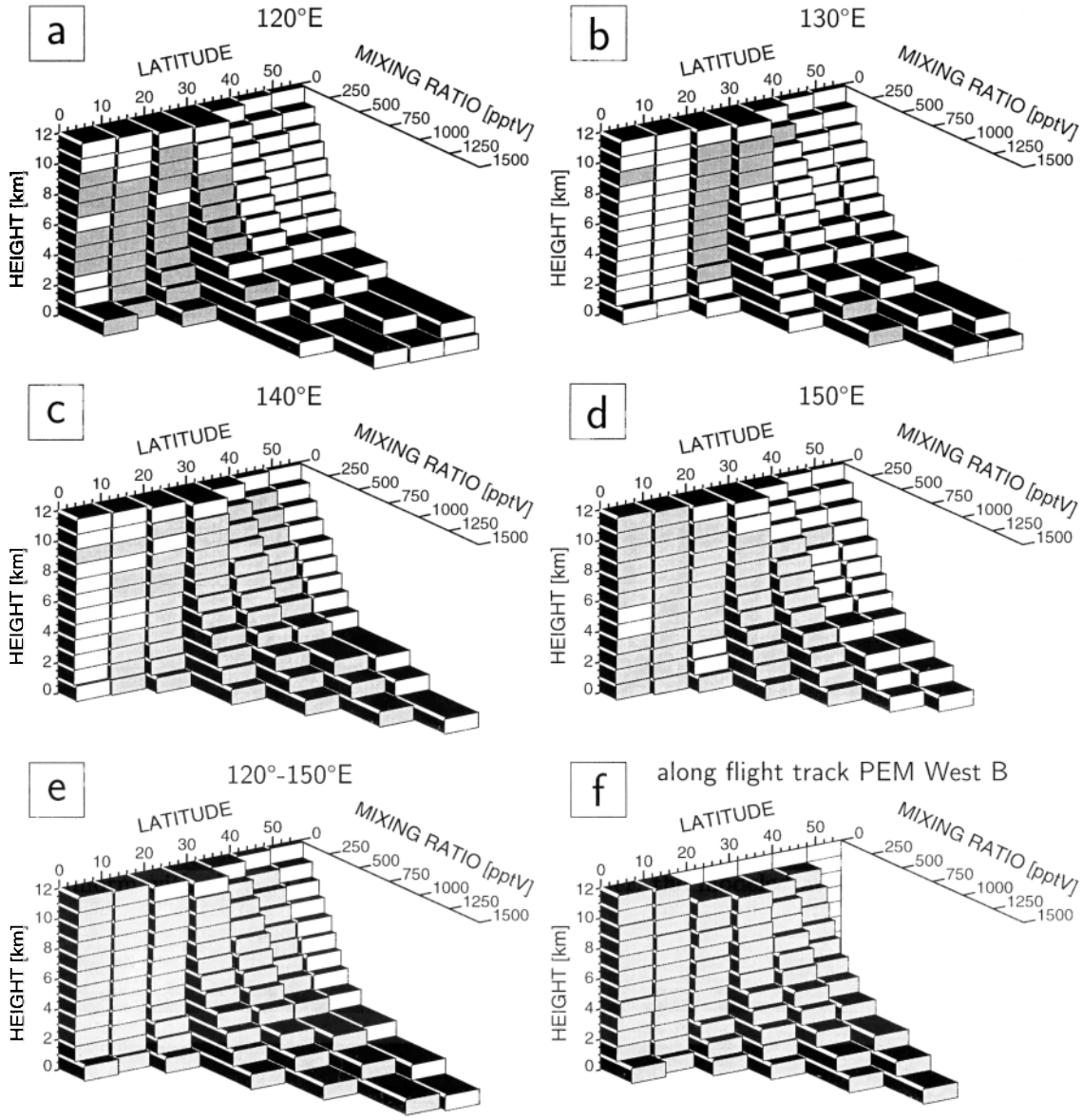

Figure 5. Altitude by latitude plots of the calculated Rn-20 mixing ratios averaged over the month of March: (a) 120°E, (b) 130°E, (c) 140°E, and (d) 150°E; (e) complete average over all longitudes; (f) average from sampling the monthly averaged distribution along the flight track. Shaded boxes were sampled at least once during the aircraft campaign PEM-West B.

tical profiles north of 30°N latitude strongly decrease with altitude over the full height range, the vertical decrease in September is limited to the lowest 3 km of the troposphere. Above that altitude the mixing ratio begins to increase in all profiles except those north of 48°N. Moreover, above the ocean this vertical increase in mixing ratio reaches to the surface layers. Relative to the surface values, the mixing ratios in the upper and midtroposphere are considerably higher during September than during March, a consequence of the more active midlatitude convection and the slower horizontal advection in the lower layers during summer. Altogether, in September the trace gas distributions are much more uniform with altitude than in March.

3.3. Sampling Bias

Contrary to the modeled tracer distributions, for which data are available at all times and for each grid box, the actual trace gas distributions during the PEM-West aircraft campaigns were sampled much more infrequently and irregularly. Although 1137 alkane measurements were made in the domain, during PEM-West A, and 1517 were made during PEM-West B, some grid boxes could be sampled only once during the campaigns and others not at all as indicated by the unshaded surfaces in Figures 4-7.

On the other hand, in each case, March and September, the modeled altitude by latitude distributions

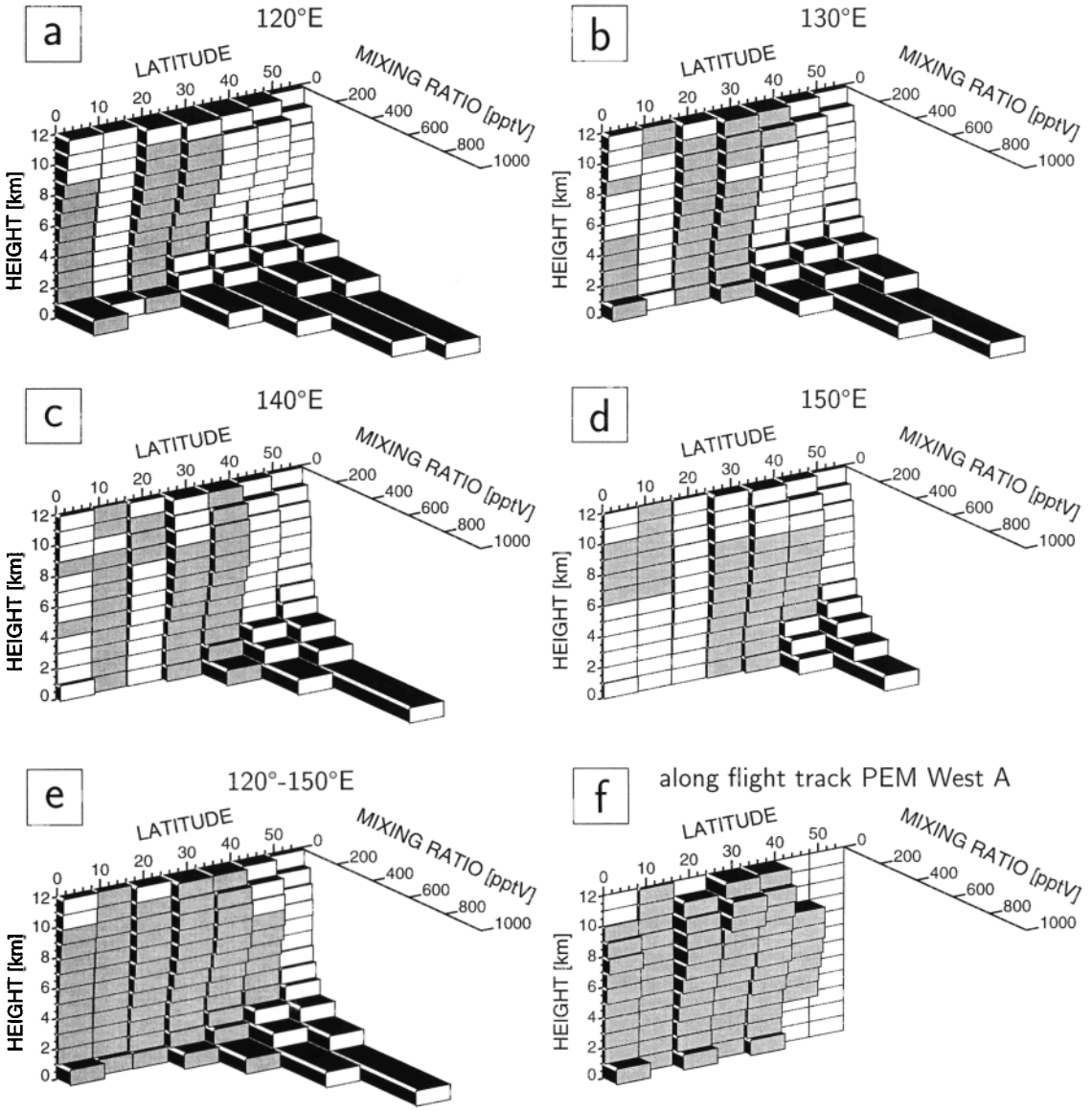

Figure 6. Altitude by latitude plots of the calculated Rn-5 mixing ratios averaged over the month of September: (a) 120°E, (b) 130°E, (c) 140°E, and (d) 150°E; (e) complete average over all longitudes; (f) average from sampling the monthly averaged distribution along the flight track. Shaded boxes were sampled at least once during the aircraft campaign PEM-West A.

along the various longitudes are similar in structure. The average over all longitudes retains this structure, and with it we obtain a fully sampled altitude by latitude distribution for each synthetic tracer and month for later comparison with observations. The respective longitudinal averages are shown as panel e of Figures 4-7. They portray quite clearly the differences between the March and September distributions just discussed.

Of course, the irregular sampling can also be simulated by the model. A first approximate step in this direction is presented in panels f of Figures 4-7. Here, for each alkane sample taken along the actual flight tracks, a model tracer value is selected from the appropriate grid box, but from the monthly averages shown in panels a-d rather than at the individual measurement times. To compare with panel e, these selected model data are also averaged over longitude. Already in this case of approximate sampling, the resulting distributions are more noisy and differ in details from the true average distributions obtained from the full set of data. Somewhat more serious is the fact that some latitudes are not covered at all by the flight track. This is the case for the lower altitudes north of 40°N in PEM-West A. As a consequence, the high surface values at northern midlatitudes are missing in the average along the flight track. This tends to emphasize the difference between the March and September distributions (panels f) when compared to the full averages (panels e). Thus, the approximately sampled tracer distributions exhibit strong vertical and latitudinal gradients in March, whereas the

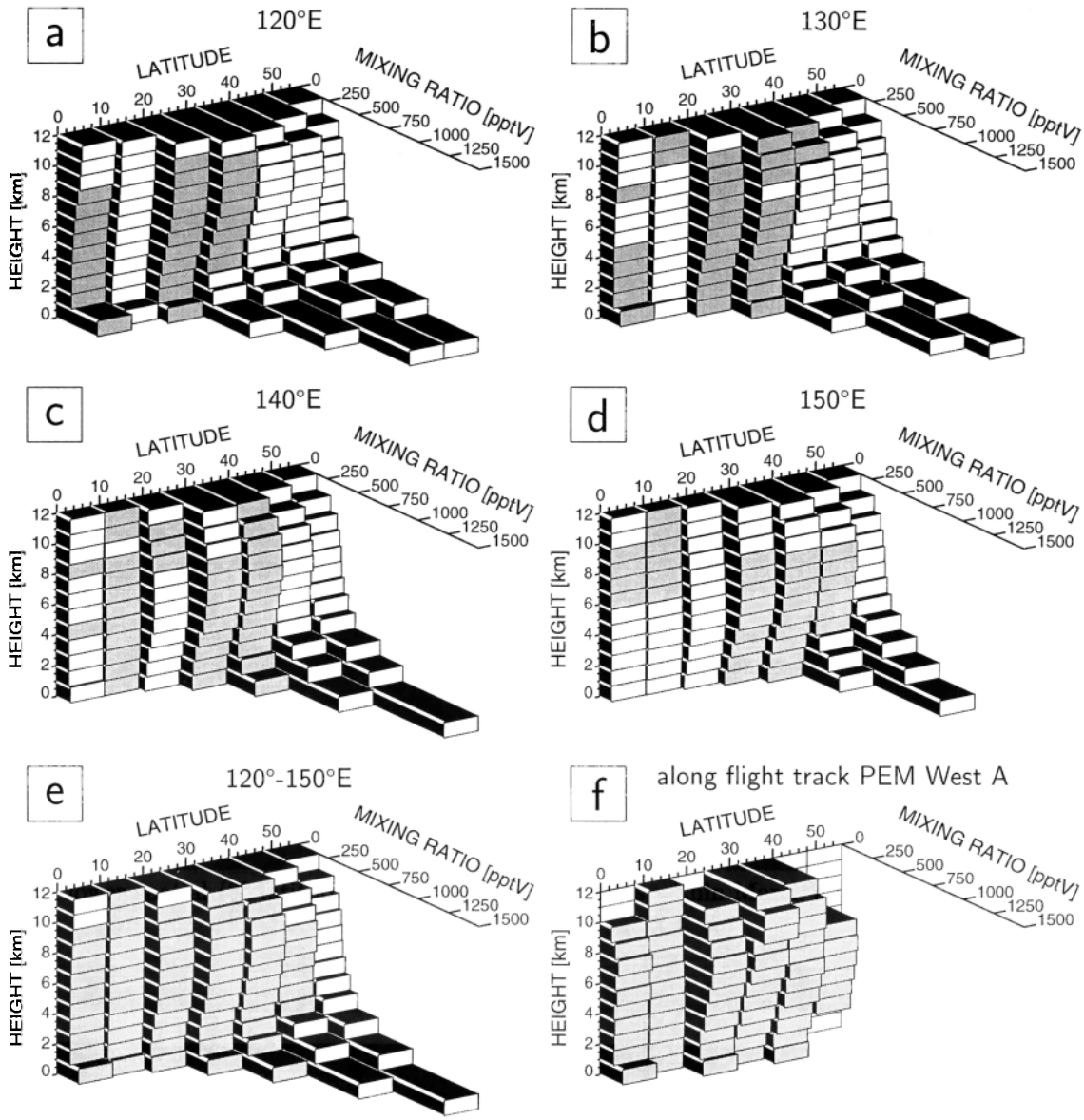

Figure 7. Altitude by latitude plots of the calculated Rn-20 mixing ratios averaged over the month of September: (a) 120°E, (b) 130°E, (c) 140°E, and (d) 150°E; (e) complete average over all longitudes; (f) average from sampling the monthly averaged distribution along the flight track. Shaded boxes were sampled at least once during the aircraft campaign PEM-West A.

ones for September show virtually no large-scale gradients in either direction. Nevertheless, where they overlap, the distributions obtained from sampling the model along the flight track are quite similar to those obtained from complete averaging.

3.4. Comparison Between Calculated Rn-5 and Rn-20 and Measured Propane and Ethane Distributions

The simplest way of intercomparing the calculated and measured trace gas distributions is to compare the sequence of their mixing ratios along the flight tracks ordered in time. This is done in Figures 8 and 9 for Rn-20 and ethane. We note that the calculated mixing ratios have a much lower spatial (8° latitude x 10° longitude x 50 hPa pressure altitude) and temporal (24 hours) resolution than the measured ones, which have about 1 km horizontal, 0.1 km vertical, and 1 min temporal resolution. Thus, as long as the flight track remains in one grid box of the given dimensions, the calculated mixing ratios will remain the same, whereas the measured ones follow the actual structure of the atmosphere. Nevertheless, the measured time sequence of ethane during PEM-West B (February 7 to March 19, 1994) and the calculated one for Rn-20 for the same time interval are highly correlated (Figure 8). A good correlation is also found for the corresponding propane and Rn-5 time sequences. In fact, both correlations remain good even when the models time interval is shifted, as long as it remains within March and April. As Table 1 indicates,

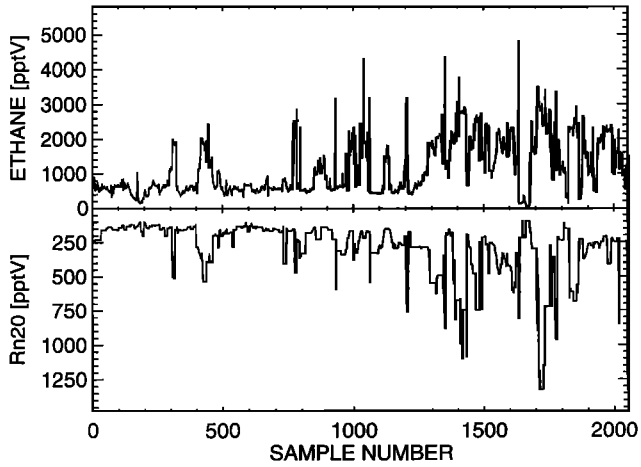

Figure 8. (top) Time sequence of the ethane mixing ratio measured during PEM-West B and (bottom) of modeled Rn-20 sampled on the same days and at the same grid box locations. For better comparison, the ordinate for Rn-20 is inverted and scaled to match the amplitudes of the variations in ethane.

Rn-5 and propane, and Rn-20 and ethane are correlated with linear correlation coefficients of 0.78 and 0.80, respectively. This result is all the more remarkable since measured propane and ethane, which are thought to have a similar source distribution and, apart from their different lifetimes, the same fate in the atmosphere, correlate with a coefficient only slightly better, namely 0.87. The high correlation between Rn-20 and ethane cannot be produced by chance, but must mean that the modeled 3-D distribution of Rn-20 and the measured distribution of ethane have a similar spatial structure over the observed domain.

In contrast, the time sequence measured for ethane during PEM-West A (September 21 to October 17, 1991) and the one calculated for Rn-20 for that time interval are not well correlated (Figure 9). The corresponding correlation coefficient is only 0.4. The same is true for the correlation between Rn-5 and propane with a correlation coefficient of 0.3. The reasons for that lack of correlation will be discussed later, after the investigation of the measured 3-D distributions of ethane and propane.

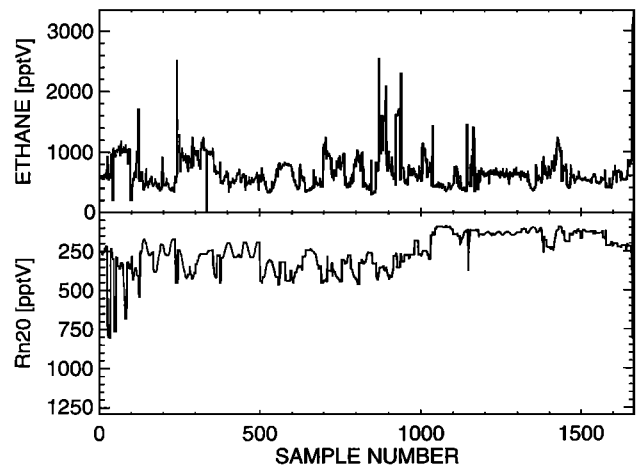

Figure 9. (top) Time sequence of the ethane mixing ratio measured during PEM-West A and (bottom) of modeled Rn-20 sampled on the same days and at the same grid box locations. For better comparison, the ordinate for Rn-20 is inverted and scaled to match the amplitudes of the variations in ethane.

Table 1. Linear Correlation Coefficients Between the Sequences of Propane and Ethane Measured During PEM-West A and B and the Corresponding Sequences of Rn-5 and Rn-20 Calculated From the Model

	PEM-West B		PEM-West A	
	Ethane	Propane	Ethane	Propane
RN-5		0.78		0.3
Rn-20	0.8		0.4	
Ethane		0.87		0.74

To better understand the good correspondence between the sequences of ethane and propane from PEM-West B and the calculated time sequences of Rn-20 and Rn-5, we will analyze the measured and calculated distributions in more detail. (Figures 10 and 11 for PEM-West B and Figures 12 and 13 for PEM-West A). In all these figures the grid box values given are the averages over all the observations in that spatial interval during the campaign. For PEM-West B, Figure 10 indicates a clear correspondence between the synthetic tracer Rn-20 and its measured counterpart ethane. The large-scale features pointed out in the model results of Figure 5 remain present with the sparser temporal subsampling. They are also visible in the experimental results: modeled and measured profiles show a decrease in mixing ratio with height north of 24°N latitude throughout the full altitude range. The decrease in the measured profiles, however, is more gradual but also more irregular than the calculated ones. A more gradual vertical decrease for ethane is not unexpected. Its lifetime increases substantially with altitude which allows relatively more tracer to arrive with the continental outflow in the upper troposphere than for the synthetic tracer Rn-20 with a constant lifetime. South of 24°N, modeled and measured mixing ratios are lower and show little vertical gradient. The tongue of elevated mixing ratios between 20°N to 40°N latitude which was clearly visible in the model distributions with full data coverage is indicated only weakly in the subsampled model distributions and hardly visible at all in the experimental results. Even the general decrease in concentration toward the east is difficult to discern in the modeled data, a result of the limited coverage and increased noise introduced by the sparser sampling. A similar behavior is found for the tracer pair Rn-5/propane.

Averaging the data contained in Figure 10 over all longitudes removes some of that noise and fills most of

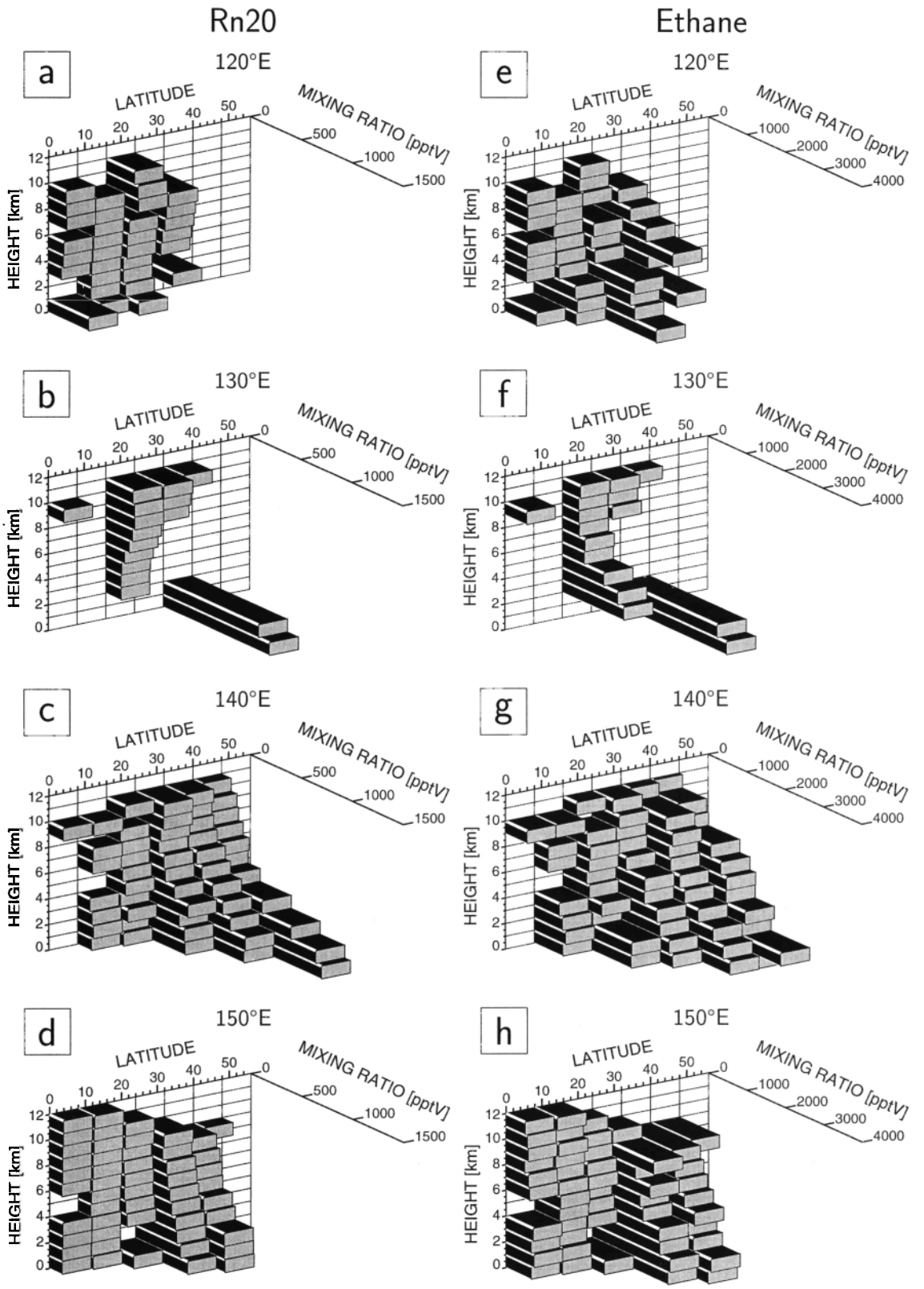

Figure 10. (e-h) Comparison of the altitude by latitude distributions of ethane measured during PEM-West B and (a-d) the modeled Rn-20 distributions sampled at the same days and grid box locations as the measured ones. Figures 10a and 10e refer to 120°E, Figures 10b and 10f refer to 130°E, Figures 10c and 10g refer to 140°E, and Figures 10d and 10h refer to 150°E longitude.

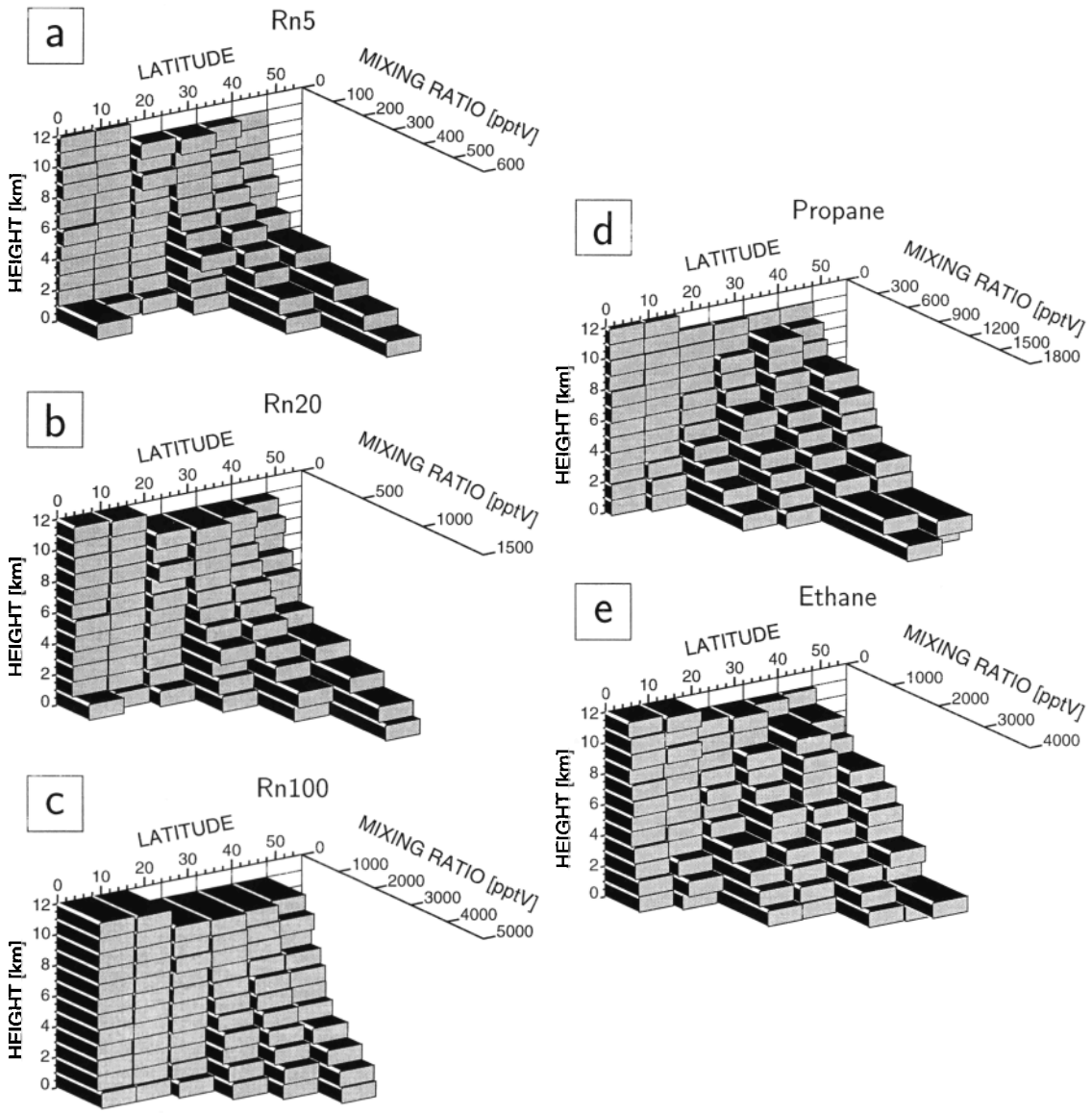

Figure 11. (d and e) Altitude by latitude distributions of propane and ethane measured during PEM-West B and averaged over all longitudes from 115°E to 155°E. (a-c) The corresponding average distributions of Rn-5, Rn-20, and Rn-100 from sampling the modeled mixing ratios on the same days and at the same locations.

the gaps. This is demonstrated by the mean distributions in Figure 11 which exhibit a remarkable agreement between the patterns in the distribution of the modeled tracers Rn-5, Rn-20, and even Rn-100 and measured trace gases, propane and ethane. There remains, of course, a large difference in absolute concentrations for both pairs Rn-5/propane and Rn-20/ethane. That difference could be reconciled by selecting a higher emission rate in the model calculations for March.

For PEM-West A the restricted sampling (Figure 12) also retains the large-scale features found in the complete model averages of Figure 7. Moreover, these features are also found in the measured data which exhibit rather uniform mixing ratios with altitude, with an occasional profile slightly increasing with altitude. The correspondence between Rn-5 and propane is similarly good, except that propane shows a very high value in the surface box at 32°-40°N and 140°E which is not seen in Rn-5. The high propane concentrations were encountered during the approach and takeoff from the Tokyo airport and are presumably due to the use of liquefied petroleum gas in its neighborhood [*Blake et al.*, 1996]. When averaged over all longitudes of the domain (see Figure 13), the altitude by latitude distribution of ethane exhibits a remarkable similarity to that of Rn-20, or Rn-100 in the sense that all these distributions are essentially flat, without the strong and coherent vertical and latitudinal gradients found during PEM-West B. On the whole, that similarity is also present for the pair propane/Rn-5.

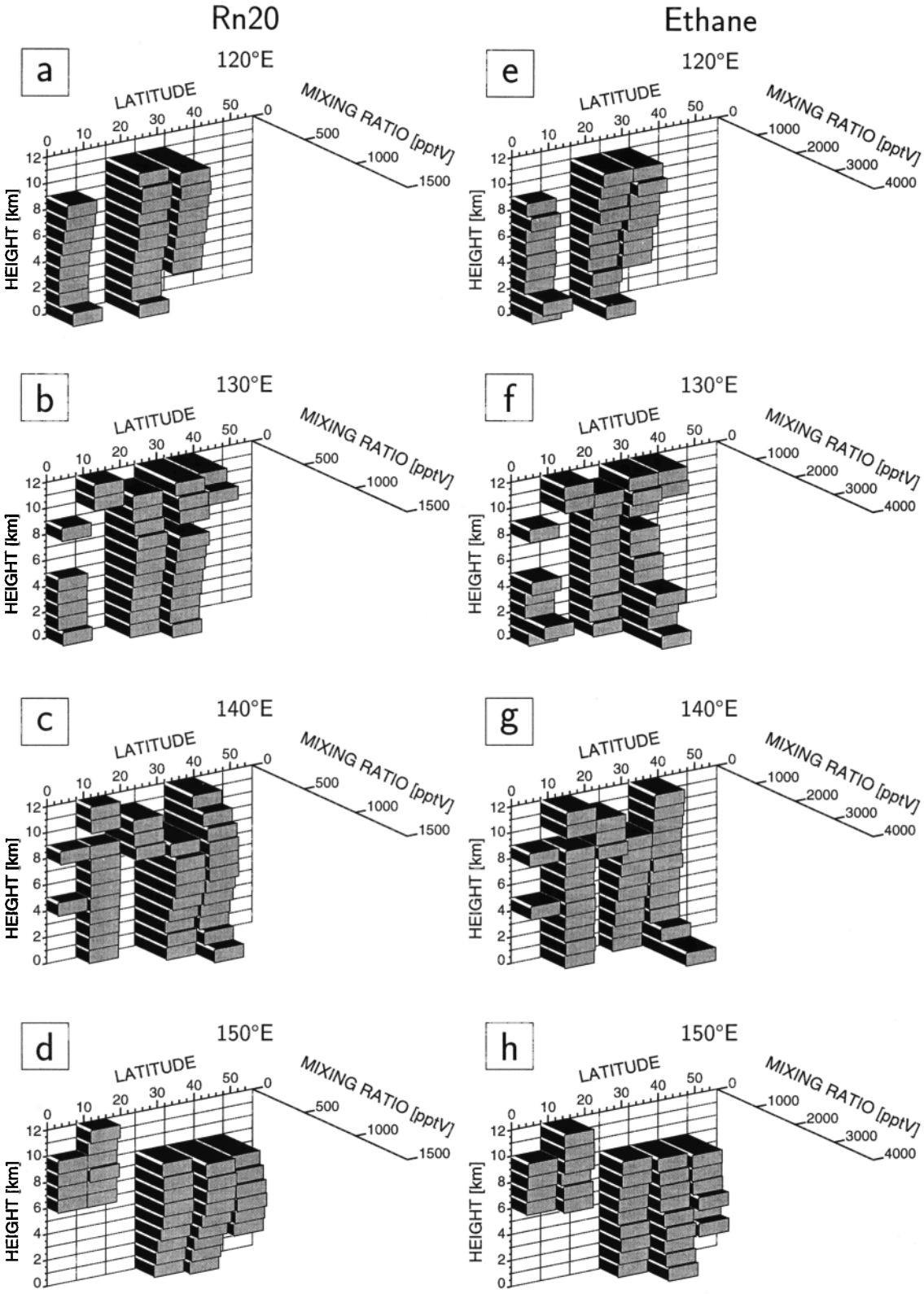

Figure 12. (e-h) Comparison of the altitude by latitude distribution of ethane measured during PEM-West A and (a-d) the modeled Rn-20 distribution sampled at the same days and grid box locations as the measured ones. Figures 12a and 12e refer to 120°E, Figures 12b and 12f refer to 130°E, Figures 12c and 12g refer to 140°E, and Figures 12d and 12h refer to 150°E longitude.

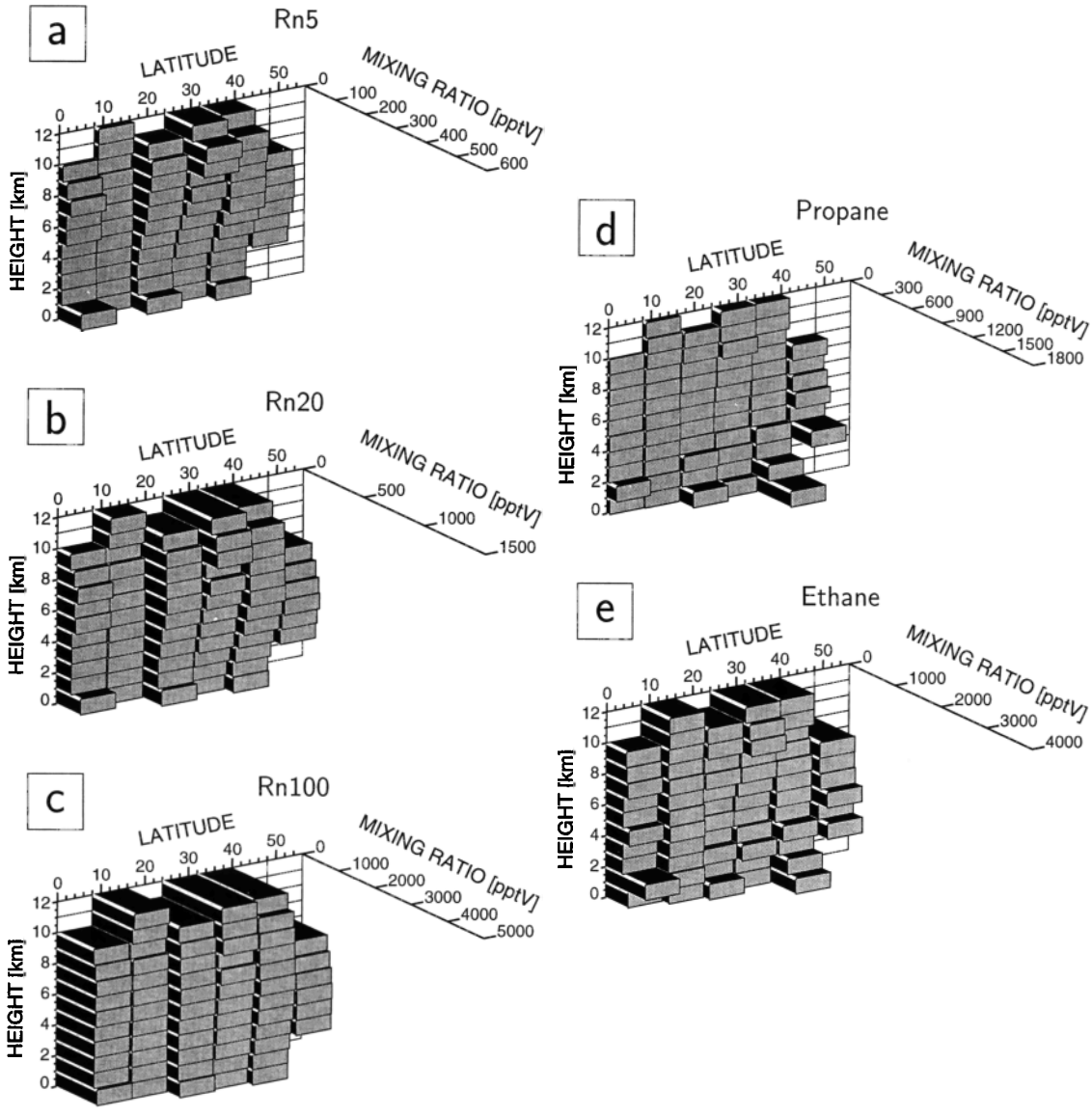

Figure 13. (d and e) Altitude by latitude distributions of propane and ethane measured during PEM-West A and averaged over all longitudes from 115°E to 155°E. (a-c) The corresponding average distributions of Rn-5, Rn-20, and Rn-100 from sampling the modeled mixing ratios on the same days and at the same locations.

4. Discussion

To illustrate the agreement in structure between the measured ethane and the calculated Rn-20 distribution in a more quantitative way, we analyze the longitudinally averaged data for PEM-West B (see Figures 11b and 11e) more closely. To do so, we remove the difference in absolute mixing ratio between the two distributions by normalizing the individual grid box values in panels b and e to the mean mixing ratio averaged over the whole distribution (301 pptv for Rn-20 and 1167 for ethane).

We also calculate the normalized standard deviation of each grid box which reflects the variance within the given altitude/latitude intervals generated by the variation of the mixing ratio in time and longitude as it is sampled along the flight track. That sampling, however, is very irregular (see Figures 3 and 11), such that for many boxes, especially those which contain only few samples, not all longitudes and only short time intervals are represented in the mean and the mean standard deviation. This may lead to an underestimate of the uncertainty of the normalized mean mixing ratio in a grid box. To remedy the situation somewhat, we calculated the relative standard deviation averaged over all grid boxes and used it as a minimum standard deviation for those grid boxes containing less than five samples. It is entered into Table 2 together with the mean normalized mixing ratios for the longitudinally averaged ethane distribution during PEM-West B and the corresponding Rn-20 distribution.

Finally, to test the agreement between the two distributions, we form the difference between the respective nomalized mixing ratios in each grid box. These differ-

Table 2. Normalized Mixing Ratios and Their Standard Deviations for the Longitudinally Averaged Distributions of Ethane, Rn-20, and the Difference, Ethane - Rn-20, During PEM-West B

Altitude, km	4°N	12°N	20°N	28°N	36°N	44°N
			Ethane			
11.5	43 ± 6, *21*	51 ± 3, *9*				
10.5	48 ± 10, *2*	45 ± 11, *4*	38 ± 4, *11*	47 ± 9, *43*	21 ± 10, *24*	8 ± 4, *17*
9.5	50 ± 4, *65*	52 ± 5, *35*	41 ± 7, *27*	47 ± 10, *20*	101 ± 23, *7*	61 ± 29, *7*
8.5	45 ± 9, *3*	46 ± 9, *50*	45 ± 7, *100*	72 ± 44, *65*	114 ± 32, *49*	78 ± 15, *6*
7.5	51 ± 2, *11*	45 ± 9, *18*	50 ± 13, *14*	75 ± 25, *18*	112 ± 15, *5*	136 ± 43, *9*
6.5	52 ± 10, *17*	49 ± 10, *9*	62 ± 20, *25*	89 ± 29, *32*	113 ± 18, *20*	158 ± 28, *19*
5.5	50 ± 10, *2*	50 ± 7, *23*	56 ± 19, *22*	120 ± 29, *9*	133 ± 29, *15*	171 ± 18, *4*
4.5	49 ± 10, *1*	54 ± 6, *38*	69 ± 29, *45*	117 ± 17, *21*	148 ± 21, *15*	170 ± 15, *6*
3.5	55 ± 11, *2*	54 ± 10, *24*	109 ± 46, *33*	147 ± 22, *42*	170 ± 25, *27*	213 ± 30, *29*
2.5	57 ± 12, *1*	73 ± 32, *16*	144 ± 30, *29*	158 ± 25, *32*	198 ± 45, *30*	206 ± 39, *17*
1.5	63 ± 13, *1*	93 ± 22, *35*	161 ± 17, *9*	173 ± 10, *8*	223 ± 27, *17*	292 ± 62, *3*
0.5	64 ± 8, *18*	82 ± 26, *47*	177 ± 58, *32*	176 ± 18, *42*	238 ± 40, *48*	241 ± 12, *12*
			Rn-20			
11.5	47 ± 1, *21*	55 ± 0, *9*				
10.5	46 ± 6, *2*	52 ± 0, *4*	81 ± 15, *11*	95 ± 1, *43*	69 ± 5, *24*	32 ± 0, *17*
9.5	48 ± 5, *65*	52 ± 1, *35*	72 ± 20, *27*	93 ± 2, *20*	63 ± 2, *7*	51 ± 2, *7*
8.5	49 ± 7, *3*	54 ± 6, *50*	89 ± 26, *100*	94 ± 14, *65*	73 ± 6, *49*	46 ± 12, *6*
7.5	45 ± 5, *11*	51 ± 5, *18*	67 ± 20, *14*	93 ± 17, *18*	84 ± 8, *5*	71 ± 14, *9*
6.5	41 ± 2, *17*	51 ± 6, *9*	73 ± 10, *25*	97 ± 3, *32*	105 ± 16, *20*	91 ± 15, *19*
5.5	51 ± 7, *2*	52 ± 5, *23*	65 ± 8, *22*	104 ± 8, *9*	119 ± 19, *15*	88 ± 26, *4*
4.5	49 ± 7, *1*	48 ± 6, *38*	64 ± 9, *45*	122 ± 16, *21*	152 ± 35, *15*	127 ± 31, *6*
3.5	44 ± 6, *2*	47 ± 3, *24*	55 ± 9, *33*	161 ± 30, *42*	187 ± 40, *27*	228 ± 35, *29*
2.5	44 ± 6, *1*	46 ± 5, *16*	56 ± 9, *29*	138 ± 23, *32*	215 ± 24, *30*	321 ± 75, *17*
1.5	42 ± 6, *1*	46 ± 3, *35*	63 ± 17, *9*	156 ± 12, *8*	276 ± 46, *17*	402 ± 57, *3*
0.5	88 ± 47, *18*	64 ± 15, *47*	92 ± 40, *32*	167 ± 7, *42*	265 ± 57, *48*	421 ± 36, *12*
			Ethane - Rn-20			
11.5	-3 ± 6, *21*	-4 ± 3, *9*				
10.5	1 ± 12, *2*	-6 ± 11, *4*	-43 ± 15, *11*	-48 ± 9, *43*	-48 ± 11, *24*	-24 ± 4, *17*
9.5	2 ± 6, *65*	0 ± 5, *35*	-31 ± 21, *27*	-46 ± 10, *20*	38 ± 23, *7*	10 ± 29, *7*
8.5	-4 ± 11, *3*	-8 ± 10, *50*	-44 ± 26, *100*	-21 ± 46, *65*	40 ± 32, *49*	31 ± 19, *6*
7.5	6 ± 5, *11*	-6 ± 10, *18*	-17 ± 23, *14*	-18 ± 30, *18*	28 ± 17, *5*	65 ± 45, *9*
6.5	11 ± 10, *17*	-1 ± 11, *9*	-11 ± 22, *25*	-8 ± 29, *32*	7 ± 24, *20*	67 ± 31, *19*
5.5	0 ± 13, *2*	-1 ± 8, *23*	-8 ± 20, *22*	16 ± 30, *9*	13 ± 34, *15*	83 ± 31, *4*
4.5	0 ± 12, *1*	6 ± 8, *38*	5 ± 30, *45*	-4 ± 23, *21*	-3 ± 40, *15*	43 ± 34, *6*
3.5	11 ± 13, *2*	7 ± 10, *24*	54 ± 46, *33*	-13 ± 37, *42*	-16 ± 47, *27*	-14 ± 46, *29*
2.5	13 ± 13, *1*	27 ± 32, *16*	88 ± 31, *29*	20 ± 33, *32*	-17 ± 51, *30*	-115 ± 84, *17*
1.5	21 ± 14, *1*	47 ± 22, *35*	98 ± 24, *9*	17 ± 15, *8*	-52 ± 53, *17*	-109 ± 85, *3*
0.5	-24 ± 47, *18*	18 ± 30, *47*	84 ± 70, *32*	9 ± 19, *42*	-26 ± 69, *48*	-180 ± 37, *12*

Both normalized mixing ratios and their standard deviations are multiplied by 100 for easier reading. Italic numbers give the number of samples. For grid boxes with less than five samples the standard deviation is estimated from the relative standard deviation averaged over all grid boxes (see text).

ences are also listed in Table 2 along with their respective standard deviations. The normalized mixing ratios for Rn-20 and ethane listed in Table 2 demonstrate again the large-scale systematic patterns observed in Figure 11, namely, a decrease going from 44°N to 4°N latitude and a decrease with altitude at the latitudes between 20° and 44°N.

The gradients are substantial. In the case of Rn-20 the systematic vertical variation at 44°N latitude ranges from a normalized mixing ratio of 4.21 at the surface to a value of 0.32 at 10.5 km altitude. The individual normalized Rn-20 mixing ratios and their gradients exceed the standard deviations, σ, listed in Table 2 by a factor of 5. The same is true for the normalized ethane mixing ratios measured during PEM-West B. Here too, σ is small compared to the systematic large-scale gradients in altitude and latitude.

For the difference between the normalized mixing ratios of ethane and Rn-20, virtually all of the large-scale systematic gradients cancel. In fact the difference, ethane-Rn-20, is smaller than or comparable to the standard deviation of the difference in most boxes (47 out of 68; see Table 2). This means that the systematic large-scale spatial gradients in both distributions are reasonably similar. To quantify the variability in each distribution, we calculate the between-box variance of each; that is, $1/n \sum_{i=1}^{n} (x_i - \bar{x})^2$, where x_i refers to the normalized mixing ratio in box i, n is total

number of boxes, $\bar{x} = 1$, and each box is given equal weight. The respective values are 0.66 for Rn-20, 0.40 for ethane, E, and 0.19 for the difference E-Rn-20. Most of that variance is introduced by the systematic structures in each distribution. The within-box variances, that is, the contribution from the sum of the σ^2, are comparatively small: 0.05, 0.04, and 0.07, respectively. As expected, the between-box variance in the distribution of E-Rn-20 is reduced significantly below that in either of the normalized tracer distributions Rn-20 or ethane. Still, the former appears to retain some variance due to systematic gradients as indicated by the fact that its between-box variance is significantly larger than its within-box variance. The gradients seem, however, to be caused by medium not large-scale features, such as the very low ethane mixing ratios observed at 10.5 km altitude and 36°N to 44°N latitude where the aircraft penetrated into stratospheric air.

As a further measure of the similarity between the (normalized) distributions of Rn-20 and ethane, we determine the correlation coefficient r between them. Calculation either from the between-box variances given above [cf. *Spiegel*, 1975] or directly from the normalized mixing ratios listed in Table 2 yields r = 0.84. That value is in good agreement with the correlation coefficient of 0.8 listed in Table 1 which was derived directly from all the individual measured ethane and model-sampled Rn-20 data. The present correlation is somewhat better, presumably due to the averaging applied to the data. Since r^2 is a measure of the explained variation [*Spiegel*, 1975], between 2/3 or 3/4 of the variation found in the measured ethane mixing ratio during PEM-West B, namely, that caused by the large-scale gradients, is explained by the modeled Rn-20 distribution for March. The results of a similar analysis for the other cases are summarized in Table 3.

Because of the difficulties in obtaining an estimate of the standard deviation for boxes containing small numbers of samples, the variances in Table 3 are defined differently: the total normalized variance is derived from the sum over all individual samples, that is, $1/m \sum_{i=1}^{m}(x_i - \bar{x})^2$, where m is the total number of measurements, x_i is the normalized mixing ratio of an individual sample, and $\bar{x}$=1. The in-box normalized variance is $1/m \sum_{ij}(x_{ij} - \overline{x_j})^2$, where $\overline{x_j}$ is the normalized mean mixing ratio in box j and the x_{ij} are the normalized mixing ratios of the samples falling in box j. In this way each grid box obtains a weight corresponding to the number of samples it contains, and the numerical values of the means and variances differ slightly from those given above for ethane and Rn-20 for PEM-West B. The total variance is the sum of in-box and between-box variance.

As Table 3 indicates, the agreement between the propane and Rn-5 fields for PEM-West B is also quite good leading to a correlation coefficient of 0.87. As for ethane, a large part of the variation in the measured propane distribution, namely, about 75%, is explained by the model Rn-5 distribution, and again the agreement rests on the similarity of the large-scale structures. We note that because of the larger relative gradients, the total normalized and between-box normalized variance of propane are considerably larger than those of ethane. Moreover, the in-box variance, and, consequently, the uncertainty in the individual grid box values, is much larger than that for ethane and explains a larger share of the total variance in the distribution of the difference, propane-Rn-5, P-Rn-5.

The situation is quite different for PEM-West A. Already, the visual inspection of Figure 13 indicates rather flat distributions, that is, a lack of large-scale spatial structure, for Rn-5, Rn-20, propane, and ethane. This

Table 3. Absolute and Normalized Means as Well as Total, In-Box, and Between-Box Normalized Variances of the Longitudinally Averaged Distributions of Propane, Ethane, Rn-5, Rn-20, Propane - Rn-5, and Ethane - Rn-20 during PEM-West A and B

	Propane	Rn-5	P - Rn-5	Ethane	Rn-20	E - Rn-20
			PEM-West A			
Absolute mean	78 pptv	49 pptv		666 pptv	275 pptv	
Normalized mean	1	1	0	1	1	0
Total normalized variance	4.74	0.52	4.57	0.16	0.14	0.22
In-box normalized variance	3.80	0.16	3.39	0.12	0.03	0.11
Between-box normalized variance	0.94	0.36	1.18	0.04	0.11	0.11
Correlation coefficients	0.24			0.56		
			PEM-West B			
Absolute mean	304 pptv	67 pptv		1147 pptv	311 pptv	
Normalized mean	1	1	0	1	1	0
Total normalized variance	2.40	1.74	1.31	0.44	0.52	0.24
In-box normalized variance	0.76	0.20	0.91	0.06	0.05	0.08
Between-box normalized variance	1.64	1.54	0.40	0.38	0.47	0.16
Correlation coefficients	0.87			0.84		

For definitions see text. Also given are the correlation coefficients between propane and Rn-5, and ethane and Rn-20.

is expressed in Table 3 by significantly smaller between-box variances in the distributions of the respective normalized mixing ratio for the PEM-West A data as compared to PEM-West B. Moreover, calculation of the differences P-Rn-5, or E-Rn-20, does not reduce the between-box variance compared to that in the distributions of the normalized mixing ratios. This is due partly to the lack of large-scale systematic structure but also to the comparatively large in-box variances of the measured distributions.

That lack of large-scale structure combined with a dominance of in-box variance and a few differing small-scale features also produces poor correlations, in contrast to PEM-West B where strong and similar large-scale gradients exist in both the measured and modeled distributions and where any sampling over extended distances generates close correlations in the time sequences (Figure 8) or distributions (Figure 11 and Table 3). For the comparison of uniform and noisy concentrations fields as in the case of PEM-West A, the correlation coefficient does not provide the simple measure for similarity; it does for PEM-West B.

Nor are the Rn or alkane distributions during PEM-West A exactly uniform. Application of an f test to the ratio of the between-box normalized variance, which characterizes the deviation from a flat concentration field, and the in-box normalized variance rejects all of the distributions for PEM-West A as flat with probabilities of larger than 99%. The major reasons for that are the vertical ridge of elevated mixing ratios between 16°N and 40°N latitude in all calculated distributions and the elevated mixing ratios at low altitudes between 32°N and 40°N latitude in the measured profiles (see Figure 13). These are, however, features of small amplitude and relatively small scales; that is, horizontal and vertical gradients are small and change sign across the field of observation, hence the appearance of flatness and essential similarity between measured and modeled distributions, especially when contrasted with the concentration fields for PEM-West B. Finally, taken together, modeled and measured data for PEM-West A and B exhibit a similar and strong seasonal change in tracer distribution between spring and fall primarily in structure and to a lesser extent also in absolute concentration.

5. Discussion and Conclusions

We demonstrated basic agreement between the measured distributions of ethane and propane during the PEM-West campaigns and the correspondingly sampled synthetic tracer fields from the model simulations (Rn-5, Rn-20). We further demonstrated good agreement between the longitudinally averaged distributions of the synthetic tracers obtained from sampling along the flight track and those derived from averaging over the full set of synthetic tracer data in the domain. Taken together, this provides a strong indication that the longitudinally averaged distributions of ethane and propane derived from the data measured during PEM-West A and B are representative of the average latitudinal pattern of these trace gases between 0°N and 50°N latitude and 115°E and 155°E longitude, despite the incomplete sampling of that domain. This agreement is present for each season, which is all the more gratifying as the tracer distributions during PEM-West B and PEM-West A, that is, during the seasons of late winter and late summer, are quite different in structure.

Such agreement further implies that regional measured trace gas distributions with a sampling density like those of the PEM-West campaigns can be used to test the regional results from 3-D model calculations. In the present case the synthetic tracer distributions are based on the most simple assumptions, namely, uniform source strength over land and constant lifetime. Nevertheless, the model correctly simulates the large seasonal difference in the patterns of the mixing ratio between March and September that are found in the measured trace gas distributions. Since the trace gas distribution depends on the source distribution, removal rate, and atmospheric transport and the former two are fixed in the model, it appears that the difference between the distribution patterns in March and September must be due mainly to seasonal changes in transport in the model and in the real atmosphere as well. In fact, the model wind fields over the domain are quite different for March and September. The mean wind field during March remains quite similar across the whole troposphere and is characterized by a strong continental outflow centered around 30°N, a cyclonic flow to the north centered at the Sea of Okhotsk, and easterly flow from the ocean south of 20°N or 10°N depending on altitude. The width and strength of the continental outflow decrease with decreasing altitude: from a width of 10°N to 50°N and a maximum wind speed of 65 m s^{-1} at sigma level 7 (202 hPa) to a width of 30°N to 50°N with a maximum wind speed of 7 m s^{-1} at sigma level 1 (959 hPa). Correspondingly, the latitude band with winds from the ocean widens from 0°N to 10°N at sigma level 7 to 0°N to 16°N at sigma level 1. As it turns out, the model wind fields during March are quite close to the average tropospheric wind fields observed during the PEM-West B campaign [*Merrill et al.*, this issue].

In contrast, the mean model wind field during September is much more irregular with altitude and exhibits much lower wind speeds than during March. There is also continental outflow in the upper troposphere during September. At sigma level 7 it reaches from 20°N to north of 60°N latitude; however, its wind speeds are much lower, about 30 m s^{-1} at their maximum at 48°N. The mean air movement at the sigma level 1 on the other hand is dominated by very weak winds from the east between 0°N and 40°N latitude; north of 40°N, winds turn anticyclonically toward the northeast and blow more strongly along the coastline.

The transition between these two regimes leads to a weak anticyclone in the middle troposphere. At sigma level 5 (470 hPa) it is centered over the Pacific at about 20°N latitude and 150°E longitude.

The correspondence between the model wind field during September and the average wind field observed during PEM-West A is not as close as in the former case. However, the broad features determining the trace gas composition agree: the outflow from the continent is much weaker, shifted to the north and does not reach to the lower altitudes south of 40°N. As a result, much of the air in the domain is of oceanic origin [cf. *Merrill et al.*, this issue; *Bachmeier et al.*, 1996]. In addition, there is faster vertical transport over the continental midlatitudes during summer in the model which causes the vertical profiles in late summer to be more uniform than in late winter. Fast vertical transport was also active during the PEM-West A campaign as evidenced by the number of typhoons present. Clearly, the agreement between modeled and measured tracer distributions is not by chance but a result of similar transport in the model and the actual atmosphere. By the same token, the seasonal differences in both the measured and modeled distributions are a result of the seasonal difference in transport. Thus the present intercomparison of the longitudinally averaged distributions of longer-lived tracers will mainly test the treatment of transport in the model. We mention in passing that the model has been found to overestimate the transport into the upper troposphere over the tropical and subtropical continents, a fact which may explain some of the smaller-scale differences between the modeled and calculated vertical profiles during PEM-West A (see Figure 13).

The modeled and measured trace gas distributions explain the poor correlation between the measured and simulated sequences of the mixing ratios along the flight track during September. In that season, modeled and measured mixing ratios are rather uniform with altitude and latitude (Figure 13). Thus there are no systematic gradients which could generate a correlation between modeled and measured mixing ratio, especially with substantial noise present from incomplete sampling and natural variability. In March, however, there are strong and similar large-scale latitudinal and vertical gradients in the modeled and measured distributions (Figure 11). These produce a good correlation between the respective sampling sequences, despite the presence of noise.

The large correlation coefficients found for PEM-West B mean that about 2/3 to 3/4 of the variance in the measured mixing ratios is explained by the modeled trace gas distributions. This underlines quantitatively that our simple model goes a long way to explain the salient features of the propane and ethane distributions observed during PEM-West A and B. This, in turn, indicates that the treatment of transport and source distributions in the model represents a reasonable first approximation. Because the correlation between measured and modeled distributions is rather high already, further improvement will be hard to achieve, and it will be difficult to gauge the effect of further refinements in the model. Thus it would be difficult to study the details in the regional distribution of sources from the present intercomparison of averaged tracer fields.

In addition, we showed that good agreement between modeled and measured distribution patterns are obtained even with approximately matched tracer lifetimes, that is, inexact chemistry (see Figures 11 and 13). It will thus also be difficult to learn much about regional chemistry from such an intercomparison. Extraction of such information demands different approaches, such as a look at shorter-lived tracers or the use of assimilated meteorological wind fields and more accurate sources or trajectory analysis of the source-receptor relationship.

So far, our analysis is restricted to one specific region, but it is fair to speculate that it may do similarly well for other regions of similar extension where sufficient propane and ethane measurements are available. Extension to other gases, in particular those with a more complicated source pattern, seems worth a try.

The present intercomparison also indicates how a 3-D model could help in the design of an aircraft campaign. Such a model presents a convenient vehicle to formulate a simple hypothesis, for example, about lifetimes or source distributions, which can be tested against experiments. The model could then be used to locate those regions of the atmosphere and those seasons with large temporal and spatial gradients in trace gases that would be easy to detect and assess.

References

Bachmeier, A.S., R.E. Newell, M.C. Shipham, Y. Zhu, D.R. Blake, and E.V. Browell, PEM-West A: Meteorological overview, *J. Geophys. Res., 101,* 1655-1677, 1996.

Blake, D.R., T.-Y. Chen, T.W. Smith, C.J.L. Wang, O.W. Wingenter, N.J. Blake, F.S. Rowland, and E.W. Mayer, Three-dimensional distribution of nonmethane hydrocarbons and halocarbons over the northwestern Pacific during the 1991 Pacific Exploratory Mission (PEM-West A), *J. Geophys. Res., 101,* 1763-1778, 1996.

Gregory, G.L., and A.D. Scott, Compendium of NASA data base for the global tropospheric experiments Pacific Exploratory Mission West-B (PEM-West B), *NASA TM-110193*, Langley Res. Cent., Hampton, Va., 1995.

Hansen, J., G. Russel, P. Stone, A. Lacis, S. Lebedeff, R. Ruedy, and L. Travis, Efficient three-dimensional global models for climate studies: Models I and II, *Mon. Weather Rev., 111,* 609-662, 1983.

McKeen, S.A., S.C. Liu, E.-Y. Hsie, X. Lin, J.D. Bradshaw, S. Smyth, G.L. Gregory, and D.R. Blake, Hydrocarbon ratios during PEM-WEST A: A model perspective, *J. Geophys. Res., 101,* 2087-2109, 1996.

Merrill, J.T., R.E. Newell, and A.S. Bachmeier, A meteorological overview for the Pacific Exploratory Mission-West, Phase B, this issue.

Prather, M.J., Numerical advection by conservation of second-order moments, *J. Geophys. Res., J. Geophys. Res.,* 91, 6671-6681, 1986.

Prather, M.J., M.B. McElroy, S.C. Wofsy, G. Russel, and D. Rind, Chemistry of the global troposphere: Fluorocarbons as tracers of air motion, *J. Geophys. Res., 92,* 6579-6613, 1987.

Prinn, R.G., R.F. Weiss, B.R. Miller, J. Huang, F.N. Alyea, D.M. Cunnold, P.B. Fraser, D.E. Hartley, and P.G. Simmonds, Atmospheric trends and lifetime of trichloroethane and global average hydroxyl radical concentrations based on 1978-1984 ALE/GAGE measurements, *Science, 269,* 187-192, 1995.

Rudolph, J., The tropospheric distribution and budget of ethane, *J. Geophys. Res., 100,* 11,369-11,381, 1995.

Spiegel, M.R., *Theory and Problems of Probability and Statistics, Schaums Outline Ser.,* McGraw-Hill, New York, 1975.

D. R. Blake and F. S. Rowland, Department of Chemistry, University of California at Irvine, Irvine, CA 92717. (e-mail dblake@orion.oac.uci.edu)

D. H. Ehhalt, F. Rohrer, and A. B. Kraus, Institut für Atmosphärische Chemie, Forschungszentrum Jülich, 52425 Jülich, Germany. (e-mail f.rohrer@fz-juelich.de)

M. J. Prather, Department of Earth System Science, University of California at Irvine, Irvine, CA 92717. (e-mail mprather@uci.edu)

(Received August 5, 1996; revised May 7, 1997; accepted May 20, 1997.)